Chemical Engineering Journal 387 (2020) 123704

Contents lists available at ScienceDirect

Chemical Engineering Journal

journal homepage: www.elsevier.com/locate/cej

Optimal catalyst particle design for flexible fixed-bed CO_2 methanation reactors

Ronny Tobias Zimmermann[a], Jens Bremer[b], Kai Sundmacher[a,b,*]

[a] Otto von Guericke University Magdeburg, Chair for Process Systems Engineering, Universitätsplatz 2, 39106 Magdeburg, Germany
[b] Max Planck Institute for Dynamics of Complex Technical Systems, Dept. Process Systems Engineering, Sandtorstraße 1, 39106 Magdeburg, Germany

HIGHLIGHTS

- Optimization of catalyst particles in a fixed-bed methanation reactor.
- Optimal particle design: active particle core encapsulated by inert diffusion barrier.
- Stoichiometric and undiluted feed to industrial scale reactor is possible.
- Optimized particle-reactor system shows reduced thermal sensitivity.
- Optimized particle-reactor system is suited for dynamic and flexible reactor operation.

GRAPHICAL ABSTRACT

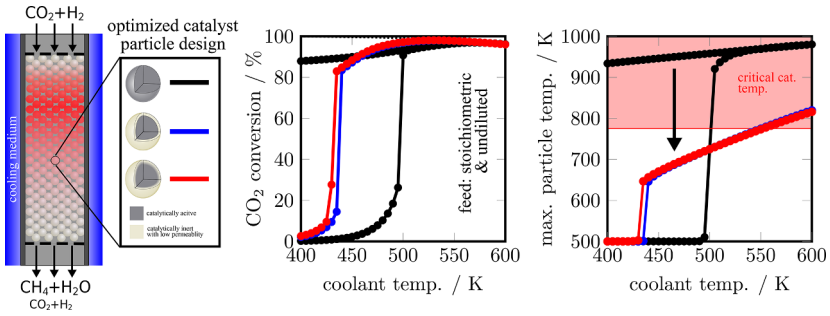

ARTICLE INFO

Keywords:
Power-to-Methane
Carbon dioxide utilization
Heterogeneous fixed-bed reactor model
Combined reactor and particle optimization
Flexible reactor operation
Egg-yolk catalyst particle

ABSTRACT

Power-to-Methane is a concept for energy storage harvested from renewable sources, for instance solar and wind power. A flexible operation of catalytic fixed-bed methanation reactors, according to the availability of energy, eliminates the need to store intermediate reactants in large buffer units. This requires reliable heat management, as the heat generation of the methanation reaction is a challenge even at steady-state conditions. For this purpose, many studies have been conducted on the reactor scale, but knowledge on how the catalyst particle design can influence reactor behavior is rather limited. Therefore, a heterogeneous reactor model is used in this study to investigate the influence of particle activity, permeability and heat conductivity on reactor performance. Subsequently, a nonlinear program is formulated and solved to find the optimal particle design depending on these three properties and their radial distribution in the catalyst particles. The designs include spherical particles with uniform properties (Case 1), particles with two uniform zones of different properties (Case 2) and particles with radially variable properties (Case 3). Optimization, subsequent sensitivity analyses and dynamic simulations reveal that reactors filled with particles of Case 2 should exhibit a particle core with high activity, which is surrounded by an inert, low-permeability shell (so-called 'egg-yolk' particles). In this way, the reactor shows a reduced parametric sensitivity and a high methane yield at the same time. In comparison to reactors filled with particles of Case 1, they also exhibit a favorable behavior for dynamic and flexible reactor operation. The benefit of further particle zones to increase reactor performance appears insignificant, as shown by the results of Case 3.

* Corresponding author at: Max Planck Institute for Dynamics of Complex Technical Systems, Sandtorstraße 1, 39106 Magdeburg, Germany.
E-mail address: sundmacher@mpi-magdeburg.mpg.de (K. Sundmacher).

https://doi.org/10.1016/j.cej.2019.123704
Received 22 July 2019; Received in revised form 17 October 2019; Accepted 3 December 2019
Available online 07 December 2019

Nomenclature

a_v	specific particle surface area $\left(\frac{1}{m}\right)$
c_p	specific heat capacity $\left(\frac{J}{kg\,K}\right)$
d	particle diameter (m)
D	reactor tube diameter (m)
D_M	molecular diffusion coefficient $\left(\frac{m^2}{s}\right)$
E_A	activation energy $\left(\frac{J}{mol}\right)$
h	heat transfer coefficient $\left(\frac{W}{K\,m^2}\right)$
$\Delta_R H$	reaction enthalpy $\left(\frac{J}{mol}\right)$
k_i	mass transfer coefficient $\left(\frac{m}{s}\right)$
k	reaction rate constant $\left(\frac{mol}{Pa\,kg_{cat}\,s}\right)$
L	reactor length (m)
M_i	molar mass $\left(\frac{kg}{mol}\right)$
t	time (s)
p	pressure (Pa)
r	particle radius (m)
R_G	gas constant $\left(\frac{J}{mol\,K}\right)$
$\Re$	reaction rate $\left(\frac{mol}{kg_{cat}\,s}\right)$
u_0	superficial gas velocity $\left(\frac{m}{s}\right)$
T	temperature (K)
U	overall heat transfer coefficient $\left(\frac{W}{K\,m^2}\right)$
x_i	mole fraction (–)
X_i	conversion (–)
y_i	mass fraction (–)
z	axial reactor coordinate (m)
α	particle mass permeability (–)
α_i	heat transfer coefficient $\left(\frac{W}{K\,m^2}\right)$
β	particle volume-related activity (–)
γ	particle heat permeability (–)
δ	dimensionless particle core radius (–)
Δ_i	diffusion volume (–)
ε	reactor bed voidage (–)
ζ	dimensionless axial reactor coordinate (–)
η	catalyst effectiveness factor (–)
Θ	particle porosity (–)
κ	switching function parameter (–)
λ	heat conductivity $\left(\frac{W}{K\,m}\right)$
Λ_R	effective radial heat conductivity $\left(\frac{W}{K\,m}\right)$
μ	viscosity (Pa s)
$\nu_{i,j}$	stoichiometric coefficient (–)
ξ	dimensionless radial particle coordinate (–)
ρ	density $\left(\frac{kg}{m^3}\right)$
σ	particle surface-related activity (–)
τ	particle tortuosity (–)
Ψ	optimization variable (–)
Φ	particle parameter (–)

1. Introduction

1.1. Power-to-Methane concept

Wind and solar power offer a renewable alternative to nuclear and fossil fuels for the production of electrical energy. However, due to their fluctuating availability, efficient storage technologies are needed. In this context, one concept is Power-to-Methane (PtM).

The key idea of PtM is to utilize electrical energy from renewable sources for hydrogen production by electrolysis of water. Subsequently, the obtained hydrogen is used for the conversion of carbon dioxide in order to produce methane, which can be used as substitute natural gas (SNG). Technically relevant carbon dioxide sources are for instance power plants, industrial processes such as steel and cement production as well as biogas plants. To avoid the integration of large reservoirs for buffering the unsteady supply of hydrogen from the electrolysis unit, it is favorable to operate the methanation reactor dynamically, according to the availability of electrical energy [1,2].

The methanation reaction is exothermic and accompanied by a reduction of total number of moles. Therefore, according to Le Chatelier's principle, the products are thermodynamically favored at low temperatures and high pressures. Gao et al. [3] give a detailed analysis of the methanation reaction thermodynamics.

$$CO_2 + 4H_2 \rightleftharpoons CH_4 + 2H_2O \quad \Delta_R H_{298K} = -164.9\ \frac{kJ}{mol}$$

Several metals are known to catalyze this reaction, amongst which nickel and ruthenium are the most prominent ones. Although the properties of a catalyst depend on many factors, ruthenium catalysts are generally seen as the most active ones. Nickel, however, is much cheaper as well as more selective and therefore often preferred. For providing a large surface area of the active components, they are usually deposited as nanoparticles on a porous support (e.g. γ-Al_2O_3). Comprehensive information about methanation catalysts is given for instance in [4–6].

1.2. Reactor concepts for methanation

Due to the thermodynamical limitation of the reaction and catalyst deactivation at high temperatures, various reactor concepts were developed in order to handle the large heat release rate of the methanation reaction, which is a challenge even at steady-state conditions. Amongst these, wall-cooled fixed-bed reactors have reached commercial application [4].

As shown by simulation studies, it is not possible to operate such reactors without a distinct hot-spot formation, when using stoichiometric and undiluted mixtures of carbon dioxide and hydrogen as feed gas, even when utilizing small tube diameters [7,8]. However, pronounced hot-spots should be avoided, as they impose a safety issue on the process and require expensive materials to operate the reactor. Due to this, many concepts have been proposed for reactor temperature control, such as feed and catalyst dilution [9,10], utilization of multiple reactors and heat exchangers in series [11] or even advanced control strategies, which exploit unstable operation points of the reactor [12]. Further concepts are discussed in [13]. While these concepts can be promising for steady-state operation, some of them exhibit unfavorable transient behavior, as shown for example by Quina and Ferreira [14] for catalyst dilution, or are coupled to an increased realization effort compared to a simple fixed-bed reactor.

Schlereth and Hinrichsen [7] point out the possibility of reactor temperature control by optimization of the interplay between mass transport, heat transport and reactions rates on the particle scale, but the potential of this approach is unexplored. Due to the large number of degrees of freedom, this is a non-trivial task for many systems under a set of given constraints, as indicated by the broad literature on this subject. For example, particles with radial distribution of the active material in the porous matrix are commonly discussed. Amongst these, 'egg-shell' particles are often favored, as they exhibit active material only close to the surface of the catalyst particles, where the reaction rates are least affected by transport resistances [1,15]. In this way, the amount of the often expensive active material in the reactor can be reduced without significant performance loss. For the opposite case

('egg-yolk' particles), the prevention of thermal runaway behavior has been reported for instance in [16]. Specifically for carbon monoxide methanation Wu et al. [17,18] have experimentally confirmed, that the carbon deposition and the selectivity can be significantly affected by the spatial distribution of the active material in the catalyst particles. In addition to the spatial distribution of the active material, the distribution of permeability and heat conductivity has also been investigated. Examples are discussed in [19,20].

1.3. Scope of this work

In order to examine the influence of the active component distribution of the catalyst particles on the thermal behavior of a fixed-bed methanation reactor, the ignition curves of a reactor filled with uniform, 'egg-shell' and 'egg-yolk' catalyst particles are compared. All of the three concepts exhibit the same total amount of activity. The most favorable distribution is further investigated with different particle activity, permeability and heat conductivity.

Subsequently, these degrees of freedom are optimized at a 'design point' in steady-state mode for three different cases, such that the maximum methane yield is obtained without surpassing the catalyst deactivation temperature, which is assumed to be 775 K [4,21]. The three cases differ by radially constant parameters, two uniform zones with different sets of parameters and radially variable parameters on the particle scale, as illustrated in Fig. 1.

In order to examine the applicability of the optimized particle-reactor systems for flexible operation, the methane yield and the maximum particle temperature are studied with respect to selected reactor parameters. The investigated parameters are the coolant temperature, as a significant parameter for controlling the reactor, as well as the inlet velocity and the reactor pressure, as possible realizations of different operation points. In addition, a start-up and a shut-down are simulated, in order to study the response of the systems to load changes.

2. Model

In order to keep the optimization problem as small as possible while still retaining the governing physical phenomena inside the reactor, a 1D-1D heterogeneous reactor model similar to the one in [22] is employed.

2.1. Reactor model

On the reactor scale, the mass and energy balance equations read as follows:

$$\frac{\partial y_{G,i}}{\partial t} = -\frac{u_0}{L\varepsilon}\frac{\partial y_{G,i}}{\partial \zeta} - \frac{a_p k_i}{\varepsilon}(y_{G,i} - y_{P,i}|_{\xi=1}), \tag{1}$$

$$\rho_G c_{p,G}\frac{\partial T_G}{\partial t} = -\frac{u_0 \rho_G c_{p,G}}{L\varepsilon}\frac{\partial T_G}{\partial \zeta} - \frac{a_p h}{\varepsilon}(T_G - T_P|_{\xi=1}) - \frac{4U}{D\varepsilon}(T_G - T_C). \tag{2}$$

In these equations $y_{G,i}$ and T_G describe the mass fraction of component i and the temperature along the dimensionless axial coordinate $\zeta = z/L$ of the reactor. The indices G, P and C denote the gas phase, the particle phase and the coolant phase, respectively. All variables are assumed constant in radial direction of the reactor and axial dispersion as well as axial heat conduction are not included in the model for the sake of simplicity. The pressure drop along the axis of the reactor is neglected and ideal behavior of the gas mixture is assumed. According to the results of previous studies, these simplifications are permissible for a qualitativ investigation of the given system [7,12,23]. Information about the calculation of the model coeffcients is given in A.1 and A.2.

2.2. Particle model

The spherical catalyst particle is described as pseudo-homogeneous system. The governing heat and mass balance equations in radial direction $\xi = \frac{r}{d/2}$ are:

$$\theta\frac{\partial y_{P,i}}{\partial t} = \frac{4}{d^2}\frac{1}{\xi^2}\frac{\partial}{\partial \xi}\left[\xi^2\frac{\theta}{\tau}D_{M,i}\frac{\partial y_{P,i}}{\partial \xi}\right] + \sigma\frac{M_i}{\rho_G}\rho_S(1-\theta)\sum_{j=1}^{N}\nu_{i,j}\Re_j, \tag{3}$$

$$(\rho c_p)_P\frac{\partial T_P}{\partial t} = \frac{4}{d^2}\frac{1}{\xi^2}\frac{\partial}{\partial \xi}\left[\xi^2\frac{1-\theta}{\tau}\lambda_S\frac{\partial T_P}{\partial \xi}\right] + \sigma\rho_S(1-\theta)\sum_{j=1}^{N}(-\Delta H_{r,j})\Re_j. \tag{4}$$

Molecular diffusion is assumed to be the main mechanism of internal mass transport, which is described according to Fick's first law. The effective molecular diffusion coefficient $D_{M,i}$ in the porous medium is calculated by scaling the bulk diffusion coefficient with the permeability, which is defined as the quotient of porosity θ and tortuosity τ of the catalyst particle. Knudsen and surface diffusion are neglected.

The effective particle heat conductivity $\lambda_P = \frac{1-\theta}{\tau}\lambda_S$ is computed according to the porous solid model [24], which neglects the heat conductivity of the fluid phase. However, as the solid heat conductivity is much larger than the fluid heat conductivity, this is a valid assumption. The particle heat capacity $(\rho c_p)_P$ is calculated by the weighted mean between gas phase heat capacity and solid heat capacity.

Heat and mass source terms are evaluated according to the reaction kinetic model proposed by Koschany et al. [25]. The equations and parameters of the model are given in A.3. The reaction rates were measured with nickel as active component distributed on an $Al(O)_x$ support in a range from 453 to 613 K and 1 to 15 bar. Only the carbon dioxide methanation reaction is taken into account in this kinetic model. In some cases, other reaction kinetic models also consider the reverse water gas shift reaction and the carbon monoxide methanation [26]. However, it has been shown, that these reactions are negligible at typical carbon dioxide methanation conditions [3,25,27]. In addition,

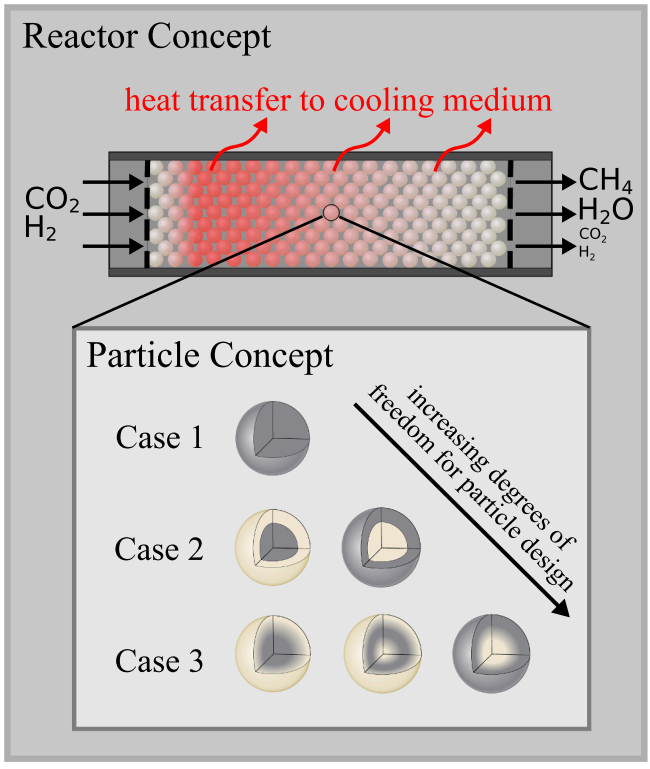

Fig. 1. Investigated catalyst particle concepts in a polytropic heterogeneous fixed-bed methanation reactor model: Case 1 – uniform parameters, Case 2 – two uniform zones with different sets of parameters and Case 3 – radially variable parameters.

even if the reactor temperature exceeds the valid range of the kinetic model of Koschany et al. [25], the amount of carbon monoxide formed is too low to qualitatively change the behavior of the reactor, as shown for example in [7,12].

In order to model the activity distribution inside the catalyst particles, the source terms are multiplied with a scaling factor σ. In practice, different activities inside the catalyst particles can be realized by varying for example the nickel surface area on the support.

To solve the model, initial and boundary conditions as well as parameters have to be supplemented. The respective model parameters are given in Table 1 and the initial as well as boundary conditions are summarized in Table 2.

Furthermore, the effective reaction rate $\mathfrak{R}_{\text{eff}}$ and the intrinsic reaction rate $\mathfrak{R}_{\text{int}}$ are defined as

$$\mathfrak{R}_{\text{eff}} = \frac{\int_0^1 (1-\theta)\sigma\mathfrak{R}\xi^2 \mathrm{d}\xi}{\int_0^1 \xi^2 \mathrm{d}\xi} \quad \text{and} \quad \mathfrak{R}_{\text{int}} = \frac{\int_0^1 (1-\theta)\sigma\mathfrak{R}_G\xi^2 \mathrm{d}\xi}{\int_0^1 \xi^2 \mathrm{d}\xi} \tag{5}$$

where $\mathfrak{R}_G$ describes the reaction rate at the conditions of the gas phase surrounding the catalyst particles. Therefore, the intrinsic reaction rate equals the reaction rate without any particle transport resistances, whereas the effective reaction rate takes these into account. The intrinsic reaction rates can vary for different catalyst particles at the same gas phase condition, due to different activity loadings.

3. Statement of the optimization problem

As nickel methanation catalysts deactivate at high temperatures, the aim of the optimization is to find values for θ, τ and σ such that an upper temperature bound is not violated, while maintaining an economical methane yield.

In order to regularize the optimization problem, the following relations are introduced:

$$\alpha = \frac{\theta}{\tau}, \quad \beta = (1-\theta)\sigma, \quad \gamma = \frac{1-\theta}{\tau}. \tag{6}$$

Substituting these relations into the particle balance equations reduces the complexity of the problem, as α and γ only appear in the respective transport terms and β solely accounts for the scaling of the source terms. In addition, the inverse relationship of τ in the transport terms is eliminated. After the optimization, α, β and γ are transformed back into θ, τ and σ.

With regard to the physical interpretation of the introduced variables, α has already been declared in the former section as permeability for mass transport of the porous medium. In this context, γ can be seen complementary as permeability for heat transport of the porous medium if the heat conductivity of the gas is neglected. Further, as σ is defined as the surface-related activity, β can be seen as a measure of the volume-related activity.

In order to find a technically realizable solution, physically meaningful bounds are given to the catalyst parameters. The lower bound for the porosity is taken as 0.05 and the upper bound as 0.5. Lower porosities would lead to numerical instabilities, whereas higher porosities could have a negative impact on the mechanical stability of the particles, especially with regard to a flexible reactor operation [32,33]. The tortuosity can be seen as factor accounting for the pore structure of the porous medium, whereas a value of one can be interpreted as perfectly straight pores. A discussion of this factor can be found for instance in [34]. The surface-related activity σ is bounded between zero and one. Zero thereby represents no active centers on the support whereas one represents the catalyst particle activity realized by Koschany et al. [25]. Furthermore, due to numerical stability reasons, an upper bound is given to β as 0.5.

It is assumed, that the thermal degradation of the catalyst starts at a temperature of 775 K [4,21]. Accounting for model inaccuracies and possible operation point changes, an additional safety margin of 50 K is included, resulting in an upper temperature limit of 725 K.

As only the methanation reaction is taken into account in the employed reaction kinetic model, the selectivity of carbon dioxide towards methane equals unity. Therefore, the yield of methane is equal to the conversion of carbon dioxide. For this reason, the target function, which is maximized, is the conversion of carbon dioxide X_{CO_2} at the reactor outlet.

The optimization problem can be summarized as follows:

$$\max_{\Psi \in \{\alpha,\beta,\gamma,(\delta)\}} X_{CO_2}(\Psi)$$

s.t. heterogeneous reactor model Eq 1-4 and Eq A.1-A.28

$$T_G(\zeta) \leqslant 725\ K$$
$$T_P(\zeta, \xi) \leqslant 725\ K$$
$$0.05 \leqslant \theta \leqslant 0.5$$
$$1 \leqslant \tau \leqslant 5$$
$$0 \leqslant \sigma \leqslant 1$$
$$0 \leqslant \beta \leqslant 0.5$$

Three cases, as illustrated in Fig. 1, are considered as possible catalyst particle configurations:

- Case 1 – constant parameters: This case represents uniform catalyst particles. It is expressed in mathematical terms as $\Psi \neq \Psi(\xi)$. The variable Ψ thereby represents any of the optimization variables.
- Case 2 – two uniform zones with different sets of parameters: This case additionally takes 'egg-shell' and 'egg-yolk' catalyst particles into account. In order to find the optimum values for each of the two zones as well as the optimum dimensionless particle core radius δ, the optimization variables α, β and γ are respectively constrained by a switching function given by:

$$\Psi = \left(\Psi_{\text{shell}} - \Psi_{\text{core}}\right)\left[0.5 + \frac{0.5(\xi-\delta)}{\sqrt{(\xi-\delta)^2+\kappa}}\right] + \Psi_{\text{core}}. \tag{7}$$

  The parameter κ, which is taken as 10^{-4}, determines the sharpness of the transition. Both κ and δ are the same for each optimization variable.
- Case 3 – radially variable parameters: In this case α, β and γ are free to be chosen by the optimization solver over the entire radius of the catalyst particles. In this case $\Psi = \Psi(\xi)$ holds.

Details on the numerical solution of the optimization problems and the simulation studies are given in Appendix B.

Table 1
Model parameters [7,28–31].

Reactor Scale			
reactor length	L	3	m
inner tube diameter	D	3	cm
particle diameter	d	2.5	mm
bed void fraction	ε	0.4	–
coolant side heat transfer coeffcient	α_{out}	500	$\frac{\text{W}}{\text{m}^2\text{K}}$
coolant temperature	T_C	500	K
superficial inlet velocity	$u_{0,in}$	1	$\frac{\text{m}}{\text{s}}$
reactor pressure	p	5	bar
Particle Scale			
solid heat capacity	$c_{p,S}$	1107	$\frac{\text{J}}{\text{kgK}}$
solid density	ρ_S	4500	$\frac{\text{kg}}{\text{m}^3}$
solid heat conductivity	λ_S	5	$\frac{\text{W}}{\text{mK}}$
Reactor Inlet State			
hydrogen mole fraction	$x_{G,H_2,in}$	0.8	–
carbon dioxide mole fraction	$x_{G,CO_2,in}$	0.2	–
temperature	$T_{G,in}$	500	K

Table 2
Model initial and boundary conditions.

Initial conditions:
reactor scale

$$y_{G,i}|_{t=0} = y_{G,i,0}$$
$$T_G|_{t=0} = T_{G,0}$$

particle scale

$$y_{P,i}|_{t=0} = y_{P,i,0}$$
$$T_P|_{t=0} = T_{P,0}$$

Boundary conditions:
reactor inlet

$$y_{G,i}|_{\zeta=0} = y_{G,i,in}$$
$$T_G|_{\zeta=0} = T_{G,in}$$

particle surface

$$\frac{\vartheta}{\tau} D_{M,i} \frac{\partial y_{P,i}}{\partial \xi}\bigg|_{\xi=1} = \frac{d}{2} k_i \left(y_{G,i} - y_{P,i} \right)$$
$$\frac{1-\vartheta}{\tau} \lambda_S \frac{\partial T_P}{\partial \xi}\bigg|_{\xi=1} = \frac{d}{2} h \left(T_G - T_P \right)$$

particle center

$$\frac{\partial y_{P,i}}{\partial \xi}\bigg|_{\xi=0} = 0$$
$$\frac{\partial T_P}{\partial \xi}\bigg|_{\xi=0} = 0$$

4. Influence of the catalyst particle design on reactor performance

To facilitate the interpretation of the optimization results, the influence of different catalyst particle concepts on the reactor behavior are examined at first. In Fig. 2 (bottom) the sensitivity analyses of the carbon dioxide conversion and maximum particle temperature in dependence of the coolant temperature are shown for different catalyst particle concepts, as this has proven to be a suitable 'fingerprint' of the thermal behavior of the reactor [7,12]. In each case, the coolant temperature is increased from 400 to 600 K and afterwards decreased again to 400 K in steps of 5 K. The concepts include uniform particles (Concept 1), with constant activity over the particle diameter, 'egg-shell' particles (Concept 2), where the active component is concentrated in the outer layer of the particles and 'egg-yolk' particles (Concept 3), where the active component is concentrated in the particle cores. Exact values are given in Table 3.

As it can be seen from the overlapping intrinsic reaction rate curves in Fig. 2 (top), all of the particle concepts exhibit exactly the same overall activity. At low temperatures, the intrinsic and effective reaction rate are the same for all three catalyst particle concepts. However, with increasing temperature, mass and heat transport resistances become more significant. Due to the varying distributions of the activity inside the catalyst particles, the effective reaction rate curves differ from the intrinsic reaction rate in different ways.

Amongst the investigated concepts, the 'egg-shell' catalyst particles are least influenced by internal mass transport resistance. In fact, there is even a section, where the effective reaction rate surpasses the intrinsic reaction rate due to heat transport resistance. The opposite is true for 'egg-yolk' particles. These particles are heavily influenced by internal mass transport resistance and the effective reaction rate deviates by several orders of magnitude from the intrinsic reaction rate at elevated temperatures. In between these two extreme cases is the effective reaction rate of the uniform catalyst particles.

The differences in the effective reaction rates result in different ignition behaviors on the reactor scale as can be seen in Fig. 2 (bottom). For all concepts, the ignition takes place at a coolant temperature of

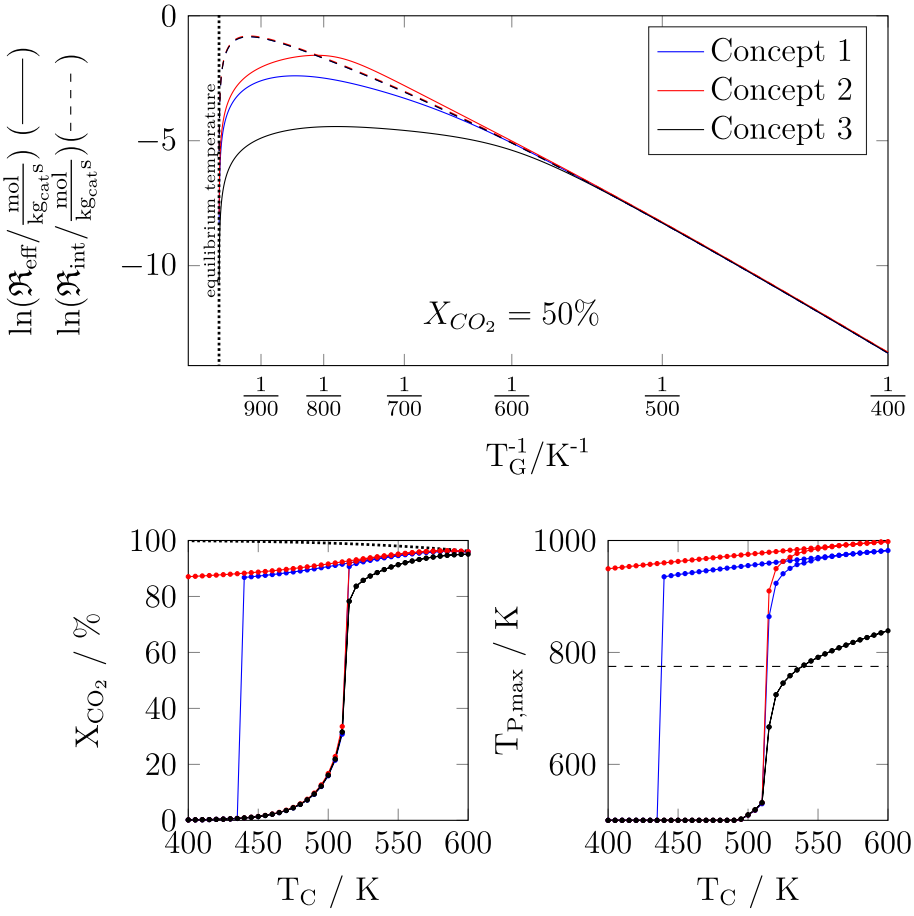

Fig. 2. Top: Arrhenius plots displaying intrinsic and effective reaction rates of different particle concepts. Bottom: Sensitivity analysis on carbon dioxide conversion and maximum particle temperature in dependence of the coolant temperature with regard to the particle design concept on the reactor scale. All parameter values used are given in Table 3.

Table 3
Investigated particle concepts for analyzing the ignition behavior of the catalytic fixed-bed reactor. Step changes for catalyst particles of Case 2 are realized by Eq. (7).

Case	1	2	2	2	2	2
Concept	1	2	3	4	5	6
Description	Uniform activity	'Egg-Shell'	'Egg-Yolk'	'Egg-Yolk'	'Egg-Yolk'	'Egg-Yolk'
Specification	–	–	reference	decr. shell heat conductivity	decr. shell permeability	incr. core activity
α_{core}	0.1250	0.1250	0.1250	0.1250	0.1250	0.1250
α_{shell}	-	0.1250	0.1250	0.1250	0.0625	0.1250
β_{core}	0.0313	0.0000	0.2500	0.2500	0.2500	0.5000
β_{shell}		0.2500	0.0000	0.0000	0.0000	0.0000
γ_{core}	0.1250	0.1250	0.1250	0.1250	0.1250	0.1250
γ_{shell}	–	0.1250	0.1250	0.0625	0.1250	0.1250
δ	–	0.9564	0.5000	0.5000	0.5000	0.5000

about 515 K and leads to a strong increase in the maximum particle temperature as well as in the conversion. For the 'egg-shell' and the uniform particles, the maximum temperature rises significantly above the assumed deactivation temperature of 775 K and both cases exhibit hysteresis behavior, which has been discussed in detail in [12]. For the 'egg-yolk' concept, the maximum temperature increase is much less pronounced, although a similar conversion as with the 'egg-shell' and uniform catalyst particles is achieved. In addition, the reactor filled with 'egg-yolk' particles shows no hysteresis behavior.

Due to these favorable features, the 'egg-yolk' concept is further investigated in three additional variations, differing by a decreased shell heat conductivity (Concept 4), decreased shell permeability (Concept 5) and increased core activity (Concept 6). The results are shown in Fig. 3.

As can be seen from Fig. 3 (top), the change in the particle parameters leads to a shift of the reaction rates. On the one hand, an increase of the activity of the catalyst particle cores leads to a higher intrinsic reaction rate (Concept 6), and therefore to higher reaction rates at low temperatures. With increasing temperature however, the effective reaction rate becomes dominated by mass transport through the particle shell. Hence, the effective reactions rates for Concept 3 and Concept 6 are almost the same at high temperatures, as they share the same parameters in the particle shell. On the other hand, a decrease of the shell permeability (Concept 5) leads to no change of the intrinsic reaction rate of the catalyst particles, and therefore to no change of the effective reaction rate at low temperatures. However, as the decreased shell permeability lowers the mass transport rate through the inert particle shell, the effective reaction rate at high temperatures is significantly decreased. The change of the heat conductivity (Concept 4) hardly affects the effective reaction rate in the investigated parameter range. For different parameters or other systems, it might have an impact, as discussed for example in [35].

The differences in the effective reaction rates are again reflected by the ignition curves of the fixed-bed reactor. An increased effective

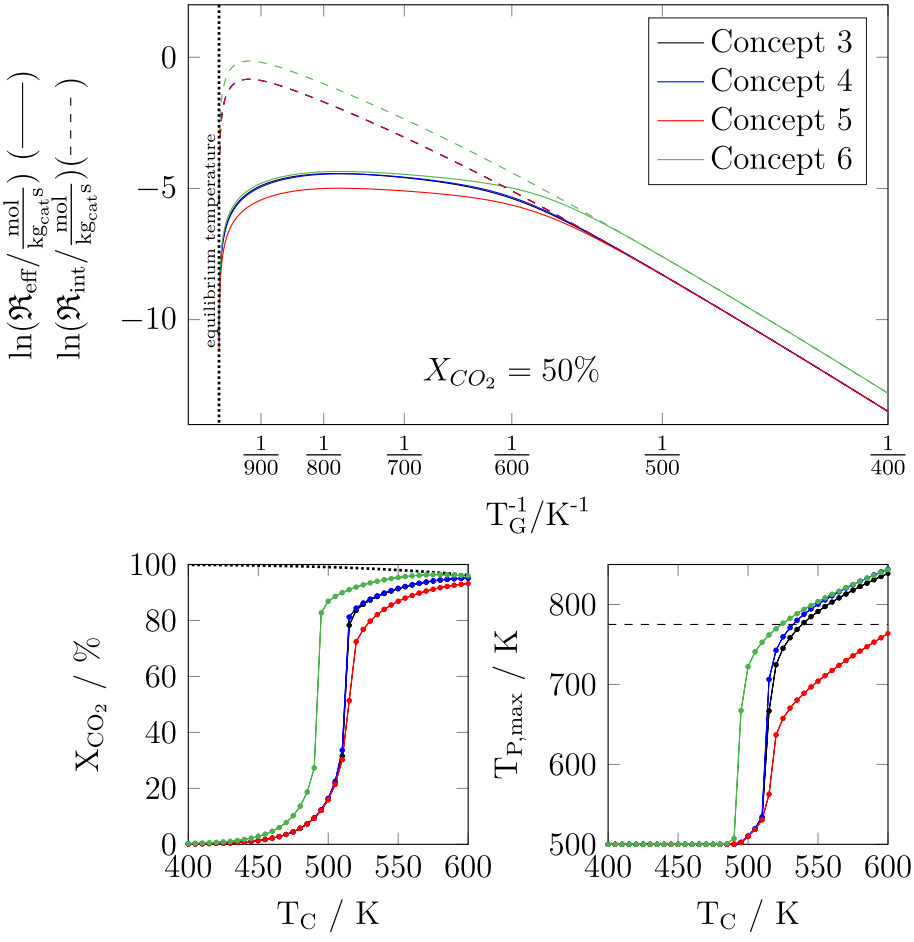

Fig. 3. Top: Arrhenius plots displaying intrinsic and effective reaction rates of different 'egg-yolk' particle concepts. Bottom: Sensitivity analysis on carbon dioxide conversion and maximum particle temperature in dependence of the coolant temperature with regard to the particle concept on the reactor scale. All parameter values used are given in Table 3.

reaction rate at low temperatures results in an ignition of the reactor at lower coolant temperatures (Concept 6). For the concept with decreased shell permeability (Concept 5), the maximum temperature is significantly decreased in the ignited reactor in comparison to the other concepts, while still achieving similar conversions.

5. Optimization results

In this section, numerical optimization is used to determine the optimal catalyst particle design with respect to the three different cases discussed in Section 3 for achieving the maximum carbon dioxide conversion at the reactor outlet without surpassing the upper temperature bound of 725 K in the reactor. This is done at a 'design-point'. It is determined by a coolant temperature of 500 K. The remaining 'design-point' parameters are displayed in Table 1. The results are shown in Fig. 4.

The lowest carbon dioxide conversion of 90.71 % is obtained in Case 1. The optimal solution includes a small volume-related activity and low permeability, but a high thermal conductivity, being realized by the minimum tortuosity and small values in surface-related activity

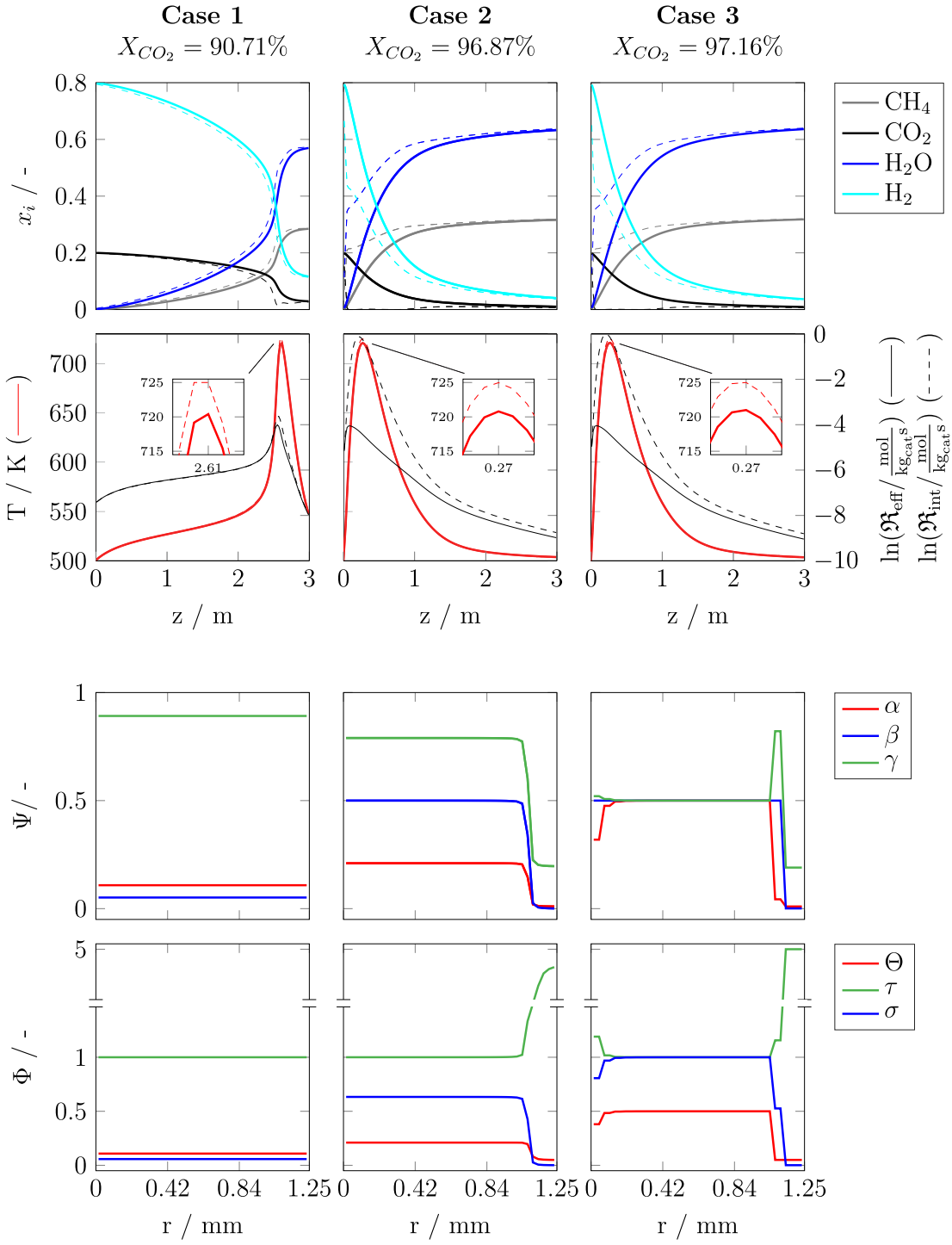

Fig. 4. Optimization Results – Top half: gas phase system state (——) and particle core system state (- - - -) at reactor scale. Additionally, the effective and intrinsic reactions rates are shown. Bottom half: Optimal solutions at particle scale.

and permeability. Despite the high reactant concentrations at the inlet of the reactor, this particle design leads to a low effective reaction rate and thereby to a comparatively slow increase of reactor temperature up to a length of about 2 m. From this length, the effective reaction rate and the temperature increase steeply. Whereas the temperature reaches its maximum in a hot-spot at 2.61 m, the effective reaction rate achieves a peak just before this length. As the gas mixture is heavily diluted by products at this point, the temperature in the particle cores remains below the upper temperature bound of 725 K. Subsequently, temperature and effective reaction rate decrease steeply towards the outlet of the reactor.

The optimal solution of Case 2 is represented by the 'egg-yolk' concept. In the shell zone, the particles exhibit no activity and low permeability. However, in the core zone of the particles, the volume-related activity is at the upper bound and the permeability is significantly higher, than in the shell zone. In addition to the mass transport resistance, a heat transport resistance is added by the shell zone of the catalyst particle as well, which increases the temperature inside the particles and thereby increases the effective reaction rate. However, as discussed in the former section, this effect seems to be negligible in the given system, as the temperature difference is at maximum 5 K at the hot spot. As seen in Fig. 5, the effective reaction rate is almost constant in the relevant temperature range. (It should be noted, that these Arrhenius plots only represent the effective reaction rates at 50 % carbon dioxide conversion.) In comparison to Case 1, the high activity of the pellet cores yields an increased effective reaction rate at low temperatures, which leads to a steep increase of temperature in the beginning of the reactor, but due to the diffusion barrier of the particle shell, the maximum effective reaction rate and therefore the maximum particle temperature is limited to 725 K. Subsequently, the effective reaction rate decreases slower than in Case 1 and a carbon dioxide conversion of 96.87 % is achieved.

The optimal solution of Case 3 is also represented by the 'egg-yolk' concept and achieves a carbon dioxide conversion of 97.16 %. As displayed in Fig. 5, the dependence of the effective reaction rate on temperature is almost identical to Case 2. Consequently, despite much more degrees of freedom, only a slight increase in carbon dioxide conversion is achieved in comparison to Case 2.

6. Reactor scale sensitivity analysis

Sensitivity analyses are performed with the obtained optimal solutions (see Section 5). The analyses include variations of coolant temperature, inlet velocity and reactor pressure. The coolant temperature is a crucial parameter for controlling the reactor and is increased from 400 to 600 K and subsequently decreased back to 400 K. Analogously, the inlet velocity from 1.5 to 0.5 m/s and the reactor pressure from 1 to 10 bar are varied. Inlet velocity and reactor pressure are possible parameters for adjusting the reactor throughput. The results are shown in Fig. 6. Infeasible states, declared as $X_{CO_2} < 90\,\%$ and $T_{P,\max} > 775$ K, are marked with a gray background. Further sensitivity studies of parameters on the particle scale are shown in Appendix C.

6.1. Coolant temperature

The sensitivity analysis of the coolant temperature (Fig. 6 (left column)) shows that the reactor starts in an extinguished state, whereby the inlet temperature represents the highest temperature in the reactor. After ignition, all three cases exhibit a carbon dioxide conversion greater than 80 %. The ignition of Case 2 and Case 3 takes place at a much lower temperature than the ignition of Case 1, due to the much higher average volume-related activity, and therefore due to a much higher effective reaction rate at low temperatures (see Fig. 5). The 'design point', which is the operation point where the optimization of the particles took place, is reached at a coolant temperature of 500 K. At this point, the highest particle temperature for all three cases corresponds to the upper bound of the optimization problem of 725 K. By increasing the coolant temperature further, the maximum particle temperature of Case 1 rises quickly above the assumed catalyst deactivation temperature of 775 K. For Case 2 and Case 3, the maximum particle temperature stays below this temperature up to a coolant temperature of 550 K.

When decreasing the coolant temperature, Case 2 and Case 3 follow the same reactor conditions as when increasing the coolant temperature. On the contrary, Case 1 depicts a hysteresis behavior and stays in an ignited state with a maximum reactor temperature of above 775 K even at a coolant temperature of 400 K. Moreover, only one single point, the 'design point', is a feasible operation state for this case. Therefore, small changes in the coolant temperature either lead to an extinction of the reactor or to thermal degradation of the catalyst. For Case 2 and Case 3 however, a whole set of feasible operation points can be observed, which makes these systems favorable for practical applications, as disturbances in the coolant temperature can be tolerated to a certain degree.

6.2. Inlet velocity

In the sensitivity analysis of the inlet velocity (Fig. 6 (middle column)), Case 1 starts in an extinguished state at a velocity of 1.5 m/s. As the axial and radial heat transport decrease with declining inlet velocity, the reactor of Case 1 ignites at the 'design point' with an inlet velocity of 1 m/s. The maximum particle temperature and the conversion increase by further decreasing the inlet velocity to 0.5 m/s. Increasing the velocity back to 1.5 m/s from 0.5 m/s, however, does not extinguish the reactor. The reactor stays in an ignited state and the maximum particle temperature rises even further. In addition, all of the ignited states except from the 'design point' are not in the feasible operation region. Therefore it can be concluded, that this case is not suited for dynamic load changes by variation of the inlet velocity. The opposite is true for Case 2 and Case 3. Here, carbon dioxide conversion is above 90% and the maximum temperature in the reactor is below 775 K for all investigated points. Moreover, no hysteresis behavior can be observed.

6.3. Reactor pressure

The same as for the sensitivity analysis of the inlet velocity can be concluded for Case 2 and Case 3 when changing the reactor pressure (Fig. 6 (right column)) in a range from 1 to 10 bar. Therefore, these particle-reactor systems are also suited for dynamic load changes by varying the reactor pressure. In this sensitivity analysis, the profile of Case 1 does not exhibit a hysteresis behavior as well. However, a complex ignition/extinction behavior can be identified, which is the result from the different dependencies of the heat release and heat removal rate on reactor pressure. As in the previous sensitivity analysis of Case 1, the 'design point' is the only feasible operation condition.

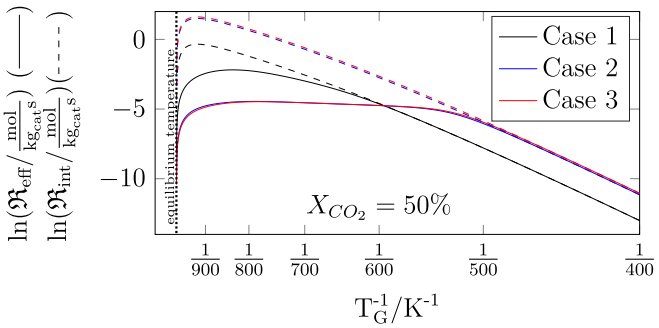

Fig. 5. Arrhenius plots displaying intrinsic and effective reaction rates of the optimized particle concepts.

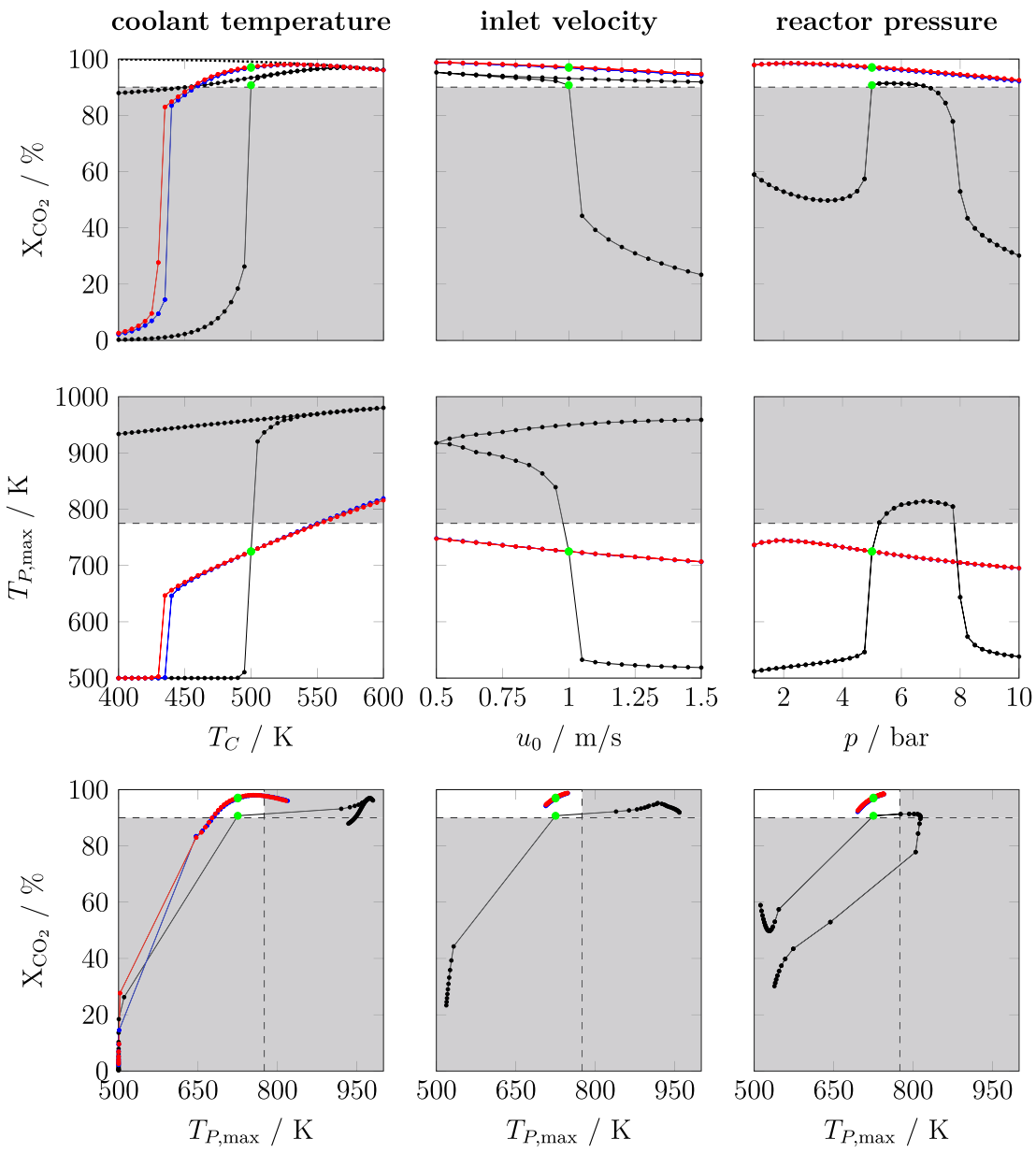

Fig. 6. Sensitivity analyses of reactor filled with the optimized catalyst particles presented in Section 5. Columnewise: coolant temperature, inlet velocity and reactor pressure. Black lines: Case 1; blue lines: Case 2; red lines: Case 3. Gray background marks areas of infeasible reactor operation points (X_{CO_2} < 90%; $T_{P,max}$ > 775 K). Green points indicate the optimized 'design point' system state of the respective case (see Fig. 4).

Therefore, this case is also unsuitable for dynamic load changes by variation of the reactor pressure.

7. Dynamic studies

A dynamic start-up and shut-down are simulated for each of the optimized cases. The initial temperature for all three particle-reactor systems is set to 300 K and the catalyst particles as well as the reactor are filled with a stoichiometric, undiluted gas mixture of hydrogen and carbon dioxide. At the beginning of the reactor start-up (t = 0 s) gas of the same composition enters the reactor with a temperature of 500 K. The coolant temperature also equals 500 K. After 3500 s, the inlet temperature and the coolant temperature are reduced to 300 K for simulating a shut-down of the reactor. The inlet composition of the gas remains the same. The remaining parameters stay unchanged and are the same as for the 'design point', which are displayed in Table 1. The results are shown in Fig. 7.

The start-up of the reactor filled with optimal particles of Case 1 takes place in essentially two steps. In the first step, the reactor interior is heated up to 500 K, while the conversion rises to about 40 %. In the second step, the reactor ignites and a conversion of greater than 90 % is obtained after 2975 s. Afterwards, the steady-state depicted in Section 5 is achieved. During the shut-down process, wrong-way behavior can be observed in the reactor, similar as in the study of Try et al. [36]. As the section in front of the hot-spot cools down, no conversion of the reactants takes place here. In consequence, the unconverted feed gas reaches the hot-spot and causes an elevation of the temperature beyond the assumed catalyst deactivation temperature of 775 K. Subsequently, the hot-spot moves out of the reactor. The extinguished steady-state is achieved after 602 s.

In comparison, the reactor filled with optimal particles of Case 2 ignites in a single step. A hot-spot is formed at the beginning of the reactor and the conversion of carbon dioxide rises above 90 % at t = 270 s. Subsequently, the steady-state shown in Fig. 4 sets in.

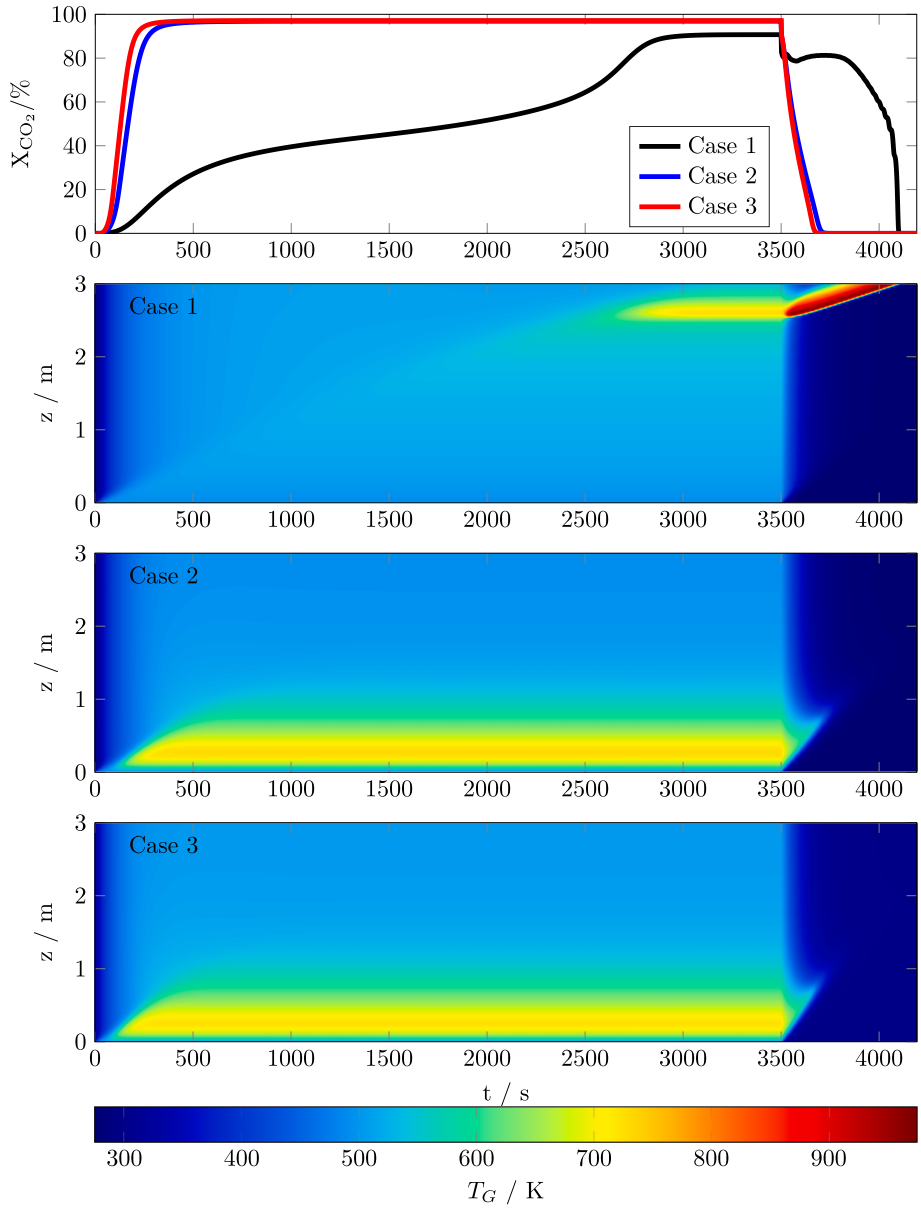

Fig. 7. Dynamic simulation results of a reactor filled with optimized particles presented in Section 5: start-up of the reactors takes place from 0 to 3500 s and shut-down from 3500 to 4200 s. The top plot shows the development of carbon dioxide conversion over time at the reactor outlet. The remaining plots show the gas temperature profile in dependence of reactor length and time for the different cases.

Despite different reactor models, the obtained start-up time is in the same order of magnitude as in [10,28]. During the shut-down of the reactor, a blow-off behavior can be observed. Hereby, the hot-spot moves along the axis of the reactor in direction of the gas stream and decreases gradually in magnitude. The extinguished steady-state is achieved after 227 s.

The behavior of the reactor filled with optimal particles of Case 3 is essentially the same, although the time for reaching a conversion of 90 % is reduced to 206 s, due to the higher porosity and therefore lower heat capacity of the particles. For the same reason, the extinguished steady-state also arises sooner as well, after 189 s.

8. Conclusion and outlook

In this work, a heterogeneous particle-reactor model has been used in order to maximize the carbon dioxide conversion of a fixed-bed methanation reactor by optimizing catalyst particle properties. Three different cases on the particle scale were distinguished:

- Case 1: uniform parameters
- Case 2: two uniform zones with different sets of parameters
- Case 3: radially variable parameters

It has been shown, that a carbon dioxide conversion of greater than 90 % is achieved in each case, while staying 50 K below of the catalyst deactivation temperature, which is assumed to be 775 K. The optimal catalyst particle concept for Case 1 is a particle with low activity and low permeability. For Case 2 and Case 3, a particle core with high activity surrounded by an inert, low-permeability shell is the best possible solution.

Dynamic simulation studies revealed that reactors filled with particles of Case 1 exhibit comparably long start-up times and wrong-way behavior when shutting down. In addition, these particle-reactor systems show a pronounced parametric sensitivity when varying the coolant temperature, the reactor pressure or the inlet velocity. In contrast, reactors filled with particles of Case 2 and Case 3 start up and shut down faster and exhibit no wrong-way behavior. These favorable

attributes for dynamic reactor operation are further highlighted in parametric sensitivity studies, where broad feasible operation regions were identified when varying coolant temperature, reactor pressure and inlet velocity. It was further shown, that Case 2 is a sufficient approximation of Case 3. Therefore, it is concluded, that the effort of preparing particles of Case 3 does not justify the negligible performance increase compared to particles of Case 2.

In summary, a fixed-bed methanation reactor filled with optimal catalyst particles of Case 2 offers the following advantages:

- Stoichiometric and undiluted feed to the reactor is possible. There is no need for feed dilution by product or inert gas in order to prevent temperatures, which cause catalyst deactivation.
- One simple fixed-bed reactor is sufficient for achieving carbon dioxide conversions of greater than 95 %. A sophisticated reactor concept, as for example with distributed feed injection or multiple reactors in series, is not necessary.
- The employed particle-reactor system shows reduced thermal sensitivity with regard to the coolant temperature and offers increased flexibility with regard to inlet velocity and pressure changes.
- A fast start-up and shut-down of the reactor is realizable. The particle-reactor concept is therefore suitable for rapid load changes.

For future work, the optimization of the catalyst particles together with the reactor design is of major interest. Additionally, the manufacturing of the proposed catalyst particle concept is an important objective, in order to experimentally validate advantages, which were discussed in this work.

Declaration of Competing Interest

The authors declare that they have no known competing financial interests or personal relationships that could have appeared to influence the work reported in this paper.

Acknowledgement

This research work was conducted within the DFG Priority Program SPP 2080 “Catalysts and reactors under dynamic conditions for energy storage and conversion” and was funded by the Deutsche Forschungsgemeinschaft (DFG, German Research Foundation) - 406914011. Ronny Zimmermann and Jens Bremer are also affiliated with the International Max Planck Research School (IMPRS) for Advanced Methods in Process and Systems Engineering, Magdeburg, Germany. (Gefördert durch die Deutsche Forschungsgemeinschaft (DFG) - 406914011.)

Appendix A. Additional model equations

A.1. Substance property models

For the heterogeneous reactor model employed in this work, the ideal gas law is used as thermal equation of state. The binary diffusion coefficients are approximated by the equation of Fuller [29]:

$$\frac{D_{i,j}}{cm^2/s} = \frac{0.00143(T/K)^{1.75}\left[\left(\frac{M_i}{g/mol}\right)^{-1} + \left(\frac{M_j}{g/mol}\right)^{-1}\right]^{1/2}}{\frac{p}{bar}\sqrt{2}\,[\Delta_i^{1/3} + \Delta_j^{1/3}]^2}. \tag{A.1}$$

The Wilke-equation [37] is used to calculate the diffusion coefficients of the mixture:

$$D_{M,i} = \frac{1 - x_i}{\sum_{j=1, i\neq j}^{N} \frac{x_j}{D_{i,j}}}. \tag{A.2}$$

Heat capacities, heat conductivities and viscosities of the pure components are calculated as given in the VDI-Wärmeatlas [29]. The latter are averaged according to the mixing rules given in [38]:

$$\lambda_G = \sum_{i=1}^{N} \frac{x_i \lambda_i}{\sum_{j=1}^{N} x_j \phi_{i,j}}, \tag{A.3}$$

$$\mu_{p,G} = \sum_{i=1}^{N} \frac{x_i \mu_i}{\sum_{j=1}^{N} x_j \phi_{i,j}}, \tag{A.4}$$

$$\phi_{i,j} = \frac{\left[1 + \left(\frac{\mu_i}{\mu_j}\right)^{0.5}\left(\frac{M_j}{M_i}\right)^{0.25}\right]^2}{\left[8\left(1 + \frac{M_i}{M_j}\right)\right]^{0.5}}. \tag{A.5}$$

The heat capacity of an ideal gas mixture is the weighted sum over the pure component mixtures:

$$c_{p,G} = \sum_{i=1}^{N} y_i c_{p,i}. \tag{A.6}$$

Reactions enthalpies are obtained by integrating the sum of the species heat capacities weighted with the stoichiometric coefficients:

$$\Delta_R H = \int_{T_0}^{T} \sum_{i=1}^{N} \nu_i c_{p,i}\, dT. \tag{A.7}$$

A.2. Transport parameters

As the density of the fluid changes in dependence of the temperature and the concentrations in reactor, the superficial velocity of the reactor is scaled according to the continuity equation:

$$u_0(\zeta) = u_{0,in}\frac{\rho_{G,in}}{\rho_G(\zeta)}. \tag{A.8}$$

For the calculation of the mass and heat flow between gas phase and catalyst particles, the specific particle surface area a_v, the respective mass transfer coefficients k_i and the heat transfer coefficient h are needed. The specific surface area of spherical catalyst particles is given by

$$a_v = 6\frac{1-\varepsilon}{d}. \tag{A.9}$$

Mass and heat transfer coefficients are calculated by the correlations of Wakao and his coworkers [39,40]:

$$k_i = \frac{D_{M,i}}{d}\left(2 + 1.1\left(\frac{\mu_G}{\rho_G D_{M,i}}\right)^{1/3}\left(\frac{u_0\rho_G d}{\mu_G}\right)^{0.6}\right), \tag{A.10}$$

$$h = \frac{\lambda_G}{d}\left(2 + 1.1\left(\frac{c_{p,G}\mu_G}{\lambda_G}\right)^{1/3}\left(\frac{u_0\rho_G d}{\mu_G}\right)^{0.6}\right). \tag{A.11}$$

The coolant temperature T_C is approximated as constant value and the overall heat transfer coefficient U lumps the heat transfer resistance at the inside (α_{in}) and outside (α_{out}) of the tube:

$$U = \left(\frac{1}{\alpha_{\text{out}}} + \frac{1}{\alpha_{\text{in}}}\right)^{-1}. \tag{A.12}$$

The heat transfer resistance of the tube wall is neglected and the heat transfer coefficient of the coolant is assumed constant. Froment [41] gives a relationship of the inner heat transfer coefficient in dependence of the effective radial heat conductivity of the fixed-bed Λ_R, the wall heat transfer coefficient to the tube wall α_{wall} and the tube diameter D:

$$\alpha_{in} = \left(\frac{1}{\alpha_{\text{wall}}} + \frac{D}{8\Lambda_R}\right)^{-1}. \tag{A.13}$$

The effective radial heat transfer coefficient in the fixed bed reactor is calculated according to the correlation of Yagi and Kunii [42]. It describes a additive superposition of the packed-bed with stagnant gas λ_{bed} and the heat transport caused by dissipative cross-mixing:

$$\Lambda_R = \lambda_{bed} + \frac{u_0\rho c_{p,G} d}{K_r} \tag{A.14}$$

In this equation K_r is an semi-empirical term for describing the flow in proximity to the tube wall. It is given for spherical particles as [29]:

$$K_r = 7\left(2 - \left(1 - \frac{2}{D/d}\right)^2\right) \tag{A.15}$$

The heat conductivity of the bed with stagnant gas is given by the model of Zehner, Bauer and Schlünder, which is explained in detail for example by Tsotsas [29]. As the Smoluchowski effect is neglected, the respective equations are:

$$\lambda_{bed} = k_{bed}\lambda_G \tag{A.16}$$

$$k_{bed} = (1 - \sqrt{1-\varepsilon})\varepsilon[\varepsilon^{-1} + k_{rad}] + (\sqrt{1-\varepsilon})[\phi k_p + (1-\phi)k_c] \tag{A.17}$$

$$k_c = \frac{2}{N}\left\{\frac{B(k_p + k_{rad} - 1)}{N^2 k_p} ln\left(\frac{k_p + k_{rad}}{B}\right) + \frac{B+1}{2B}[k_{rad} - B] - \frac{B-1}{N}\right\} \tag{A.18}$$

$$N = 1 + \frac{k_{rad} - B}{k_p} \tag{A.19}$$

$$B = C_f\left[\frac{1-\varepsilon}{\varepsilon}\right]^{10/9} \tag{A.20}$$

$$k_{rad} = \frac{4\sigma_{rad}}{2/\varepsilon_{rad} - 1}T^3\frac{d}{\lambda_G} \tag{A.21}$$

$$k_p = \frac{\lambda_{P,o}}{\lambda_G} \tag{A.22}$$

The parameter of the model are the shape factor for spheres $C_f = 1.250$, the Stefan-Boltzmann-constant $\sigma_{\text{rad}} = 5.67 \times 10^{-8}\frac{\text{W}}{\text{m}^2\text{K}}$, the emission coefficient of the catalyst particles $\varepsilon_{\text{rad}} = 0.4$ and a flattening coefficient for spheres $\phi = 0.0077$ [29].

The wall heat transfer coefficient on the inside of the reactor wall is given by the correlation of Martin and Nilles [43]:

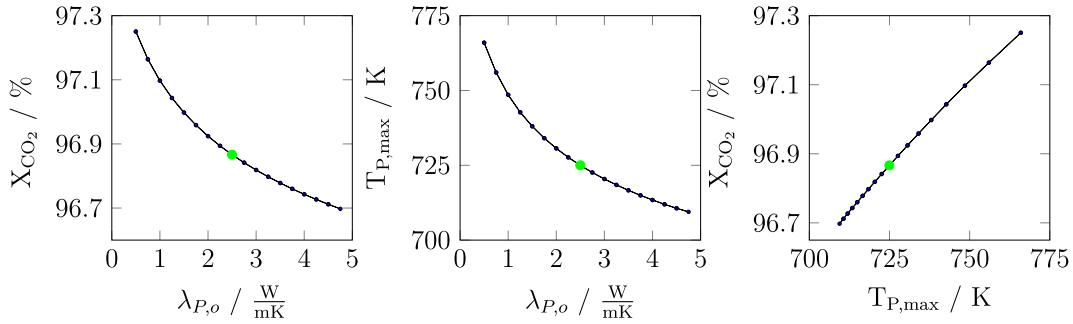

Fig. A.8. Sensitivity analysis of a reactor filled with optimized catalyst particles of Case 2 shown in Section 5 in dependence on the overall particle heat conductivity. The optimal value of Section 5 is indicated by the green dot. (For interpretation of the references to colour in this figure legend, the reader is referred to the web version of this article.)

$$\alpha_{\text{wall}} = \frac{\lambda_G}{d}\left(\left(1.3 + 5\frac{d}{D}\right)\frac{\lambda_{bed}}{\lambda_G} + 0.19\left(\frac{u_0\rho_G d}{\mu_G}\right)^{0.75}\left(\frac{c_{p,G}\mu_G}{\lambda_G}\right)^{0.33}\right) \tag{A.23}$$

The model of Zehner, Bauer and Schlünder was derived for particles with constant heat conductivity over the whole diameter. However, in this study, the heat conductivity can vary in some cases over the diameter of the particles, and therefore an overall particle heat conductivity would have to be inserted into the equations. To the best of the authors' knowledge, no such correlation exists in literature. For the studies in this work, it was therefore fixed to 2.5 $\frac{W}{mK}$, as this equals exactly half of the solid heat conductivity of 5 $\frac{W}{mK}$. To identify the influence of this parameter on the reactor performance, in Fig. A.8 a sensitivity analysis on the conversion and maximum reactor temperature in dependence of the overall heat transfer conductivity for optimized particles of Case 2 is shown. The influence of this parameter on the carbon dioxide conversion in the covered parameter range is diminishing. In contrast, it has a rather large influence on the maximum particle temperature and a low overall particle heat conductivity could lead to a severe underestimation of the maximum particle temperature. However, such a low overall particle heat conductivity is not expected, if taking the volume-averaged particle heat conductivity

$$\overline{\lambda_P} = \frac{\int_0^1 \gamma(\xi)\lambda_S \xi^2 \mathrm{d}\xi}{\int_0^1 \xi^2 \mathrm{d}\xi}, \tag{A.24}$$

which equals 2.92 $\frac{W}{mK}$, as approximation for this value.

A.3. Reaction kinetic equations

The following rate constant, adsorptions constants and equilibrium constant supplement the reaction kinetic equation of Koschany et al. (Eq A.25) together with parameters given in Table A.4 [25]:

$$\Re = \frac{k p_{H_2}^{0.5} p_{CO_2}^{0.5}\left(1 - \frac{p_{CH_4} p_{H_2O}^2}{p_{CO_2} p_{H_2}^4 K_{eq}}\right)}{\left(1 + K_{OH}\frac{p_{H_2O}}{p_{H_2}^{0.5}} + K_{H_2} p_{H_2}^{0.5} + K_{mix} p_{CO_2}^{0.5}\right)^2} \tag{A.25}$$

$$k = k_{0,555K}\exp\left(\frac{E_A}{R_G}\left(\frac{1}{T_{ref}} - \frac{1}{T}\right)\right) \tag{A.26}$$

Table A.4
Reaction kinetic parameters [25].

$k_{0,555K}$	3.46×10^{-4}	$\frac{\text{mol}}{\text{bar s g}_{\text{cat}}}$
E_A	77.5	$\frac{\text{kJ}}{\text{mol}}$
$A_{OH,555K}$	0.5	$\frac{1}{\text{bar}^{0.5}}$
ΔH_{OH}	22.4	$\frac{\text{kJ}}{\text{mol}}$
$A_{H_2,555K}$	0.44	$\frac{1}{\text{bar}^{0.5}}$
ΔH_{H_2}	−6.2	$\frac{\text{kJ}}{\text{mol}}$
$A_{mix,555K}$	0.88	$\frac{1}{\text{bar}^{0.5}}$
ΔH_{mix}	−10.0	$\frac{\text{kJ}}{\text{mol}}$
$k_{0,eq}$	137	$\frac{1}{\text{bar}^2}$
ΔG	158.7	$\frac{\text{kJ}}{\text{mol}}$
N_{eq}	−3.998	–
T_{ref}	555	K

$$A_X = A_{X,555K}\exp\left(\frac{\Delta H_X}{R_G}\left(\frac{1}{T_{ref}} - \frac{1}{T}\right)\right) \tag{A.27}$$

$$K_{eq} = k_{0,eq}\left(\frac{T}{K}\right)^{N_{eq}}\exp\left(\frac{\Delta G}{R_G T}\right) \tag{A.28}$$

Appendix B. Numerical solution strategy

To solve the simulation and optimization problems in this work, the balance equations are discretized by the Finite-Volume-Method [44]. For averaging the transport coefficients between the finite volumes, the harmonic mean is employed. The axial direction of the reactor is discretized by 150 equally spaced finite volumes, whereas the catalyst domain is discretized by 40 equally distributed finite volumes. Considering the mass balances of the four chemical species as well as the energy balances on reactor and particle scale, a nonlinear ODE system of size $n = (40 + 1)\cdot 150\cdot 5 = 30750$ is obtained. The equation system is implemented into the CasADi framework [45] in MATLAB.

To obtain feasible starting point for the optimization, the systems are integrated from an extinguished system state to steady-state, using the CVodes integrator [46]. To ensure the stationarity of the received solution, the given system is solved once more by a newton equation solver, with the given steady-state solution from the transient simulation as initial guess. The solution of the optimization problem is done by using IPOPT [47] with MA97 as underlying linear solver on a LINUX machine. In order to increase the numerical stability of Case 3, 20 degrees of freedom are used for each optimization variable in radial direction. One degree of freedom of each optimization variable therefore accounts for two neighboring finite volumes. The subsequent transient simulations and sensitivity analysis are carried out the same way as the starting guess generation for the optimization studies.

Appendix C. Particle scale sensitivity analysis

The following results extend the sensitivity analyses, which were done in Section 6, to the particle scale. It has been shown, that the particle-reactor system of Case 1 is not suited for a dynamic and flexible operation of methanation reactors. It can be further concluded, that the performance gain of the particle-reactor system of Case 3 is diminishing compared to Case 2, despite the increased realization effort. Therefore, the following studies focus on Case 2.

Due to stochastical influences during the catalyst particle production, it cannot be guaranteed that each particle corresponds exactly to the specifications of the optimization study. In order to investigate the consequences, the carbon dioxide conversion and the maximum particle temperature with respect to particle properties are analyzed. Therefore, the particle diameter and the dimensionless core radius, as well as the permeability of the shell zone and the activity of the core zone are varied.

As seen in Fig. C.9, decreasing the particle diameter and shifting the core radius towards the particle surface results in increasing carbon dioxide conversion, as both instances lead to an increase of catalyst particle activity at the loss of shell diffusion resistance. Thereby, the effective reaction rate is raised. However, this also increases the maximum particle temperature in the reactor. A certain tolerance space from the 'design point' exists, but in order to guarantee flexible reactor operation without harming the catalyst, particles with larger diameters than at the 'design point' should be preferred to smaller ones, as these do still achieve feasible carbon dioxide conversions but at lower maximum particle temperatures. For the same reason, particles with thicker inert shells should be preferred over particles with thin shells.

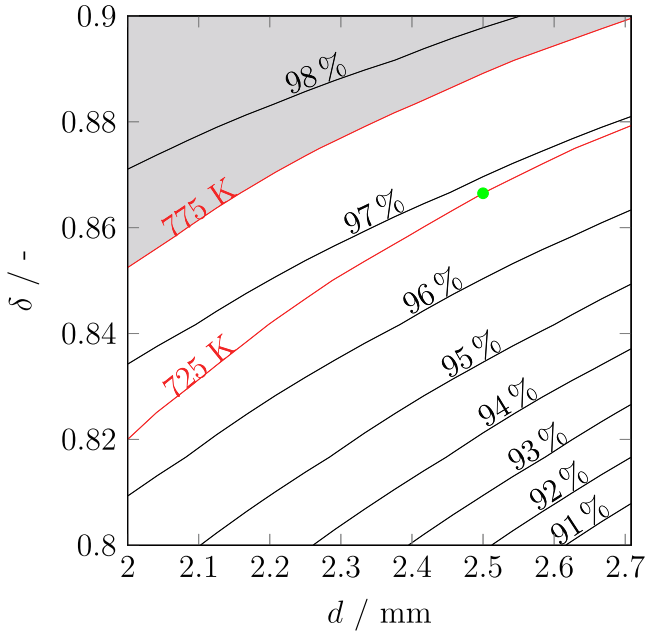

Fig. C.9. Sensitivity analysis of a reactor filled with optimized catalyst particles of Case 2 presented in Section 5. Carbon dioxide conversion (——) and maximum particle temperature (——) are shown in dependence of the particle diameter and the dimensionless core radius. Gray background marks area of infeasible reactor operation ($X_{CO_2} < 90\%$; $T_{P,max} > 775$ K). The optimal value of Section 5 is indicated by the green dot. (For interpretation of the references to colour in this figure legend, the reader is referred to the web version of this article.)

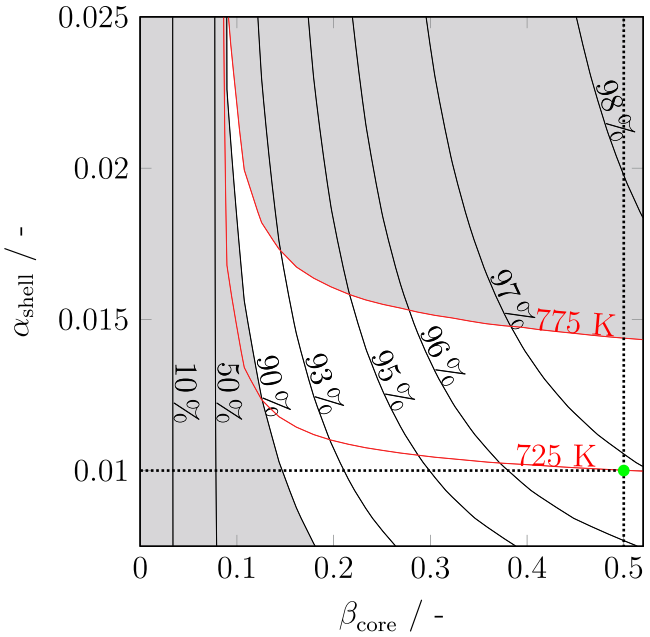

Fig. C.10. Sensitivity analysis of a reactor filled with optimized catalyst particles of Case 2 presented in Section 5. Carbon dioxide conversion (——) and maximum particle temperature (——) are shown in dependence of the volume-related core activity and shell permeability. Gray background marks areas of infeasible reactor operation points ($X_{CO_2} < 90\%$; $T_{P,\max} > 775$ K). The optimal value presented in Section 5 is indicated by the green dot. (For interpretation of the references to colour in this figure legend, the reader is referred to the web version of this article.)

Fig. C.10 indicates, that the conversion and the maximum particle temperature increase with rising volume-related activity in the particle core and with rising permeability of the particle shell. However, both of these variables vary in different ways. Starting from the 'design point', the volume-related activity can drop to a value of 0.15 before leaving the feasible operation region. This knowledge offers two opportunities for reactor design. On the one hand, it can be used in order to reduce the amount of active material in the particle, therefore lowering the catalyst costs. On the other hand, it is shown, that there is no significant performance loss to be expected by possible long term aging processes, which possibly deactivate the catalyst over an extended time period. It can be further concluded from Fig. C.10, that the permeability of the shell zone has a large impact on the maximum particle temperature. Increasing the permeability to 0.0145 from the 'design point' results in an inadmissible maximum particle temperature in the reactor. For this reason, the permeability of the shell zone should be adjusted with care when preparing the particles.

References

[1] M. Iglesias González, H. Eilers, G. Schaub, Flexible operation of fixed-bed reactors for a catalytic fuel synthesis-CO2 hydrogenation as example reaction, Energy Technol. 4 (1) (2016) 90–103, https://doi.org/10.1002/ente.201500259.

[2] K.F. Kalz, R. Kraehnert, M. Dvoyashkin, R. Dittmeyer, R. Gläser, U. Krewer, K. Reuter, J.-D. Grunwaldt, Future challenges in heterogeneous catalysis: understanding catalysts under dynamic reaction conditions, ChemCatChem 9 (1) (2017) 17–29, https://doi.org/10.1002/cctc.201600996.

[3] J. Gao, Y. Wang, Y. Ping, D. Hu, G. Xu, F. Gu, F. Su, A thermodynamic analysis of methanation reactions of carbon oxides for the production of synthetic natural gas, RSC Adv. 2 (6) (2012) 2358, https://doi.org/10.1039/c2ra00632d.

[4] S. Rönsch, J. Schneider, S. Matthischke, M. Schlüter, M. Götz, J. Lefebvre, P. Prabhakaran, S. Bajohr, Review on methanation – from fundamentals to current projects, Fuel 166 (2016) 276–296, https://doi.org/10.1016/j.fuel.2015.10.111.

[5] P. Frontera, A. Macario, M. Ferraro, P. Antonucci, Supported catalysts for CO2 methanation: a review, Catalysts 7 (12) (2017) 59, https://doi.org/10.3390/catal7020059.

[6] K. Jalama, Carbon dioxide hydrogenation over nickel-, ruthenium-, and copper-based catalysts: review of kinetics and mechanism, Catal. Rev. 59 (2) (2017) 95–164, https://doi.org/10.1080/01614940.2017.1316172.

[7] D. Schlereth, O. Hinrichsen, A fixed-bed reactor modeling study on the methanation of CO2, Chem. Eng. Res. Des. 92 (4) (2014) 702–712, https://doi.org/10.1016/j.cherd.2013.11.014.

[8] K.H. Rätze, J. Bremer, L.T. Biegler, K. Sundmacher, Physics-based surrogate models for optimal control of a CO2 methanation reactor, 27th European Symposium on Computer Aided Process Engineering, Vol. 40 of Computer Aided Chemical Engineering, Elsevier, 2017, pp. 127–132, , https://doi.org/10.1016/B978-0-444-63965-3.50023-4.

[9] S. Matthischke, R. Krüger, S. Rönsch, R. Güttel, Unsteady-state methanation of carbon dioxide in a fixed-bed recycle reactor — experimental results for transient flow rate ramps, Fuel Process. Technol. 153 (2016) 87–93, https://doi.org/10.1016/j.fuproc.2016.07.021.

[10] A. Fache, F. Marias, V. Guerré, S. Palmade, Optimization of fixed-bed methanation reactors: safe and efficient operation under transient and steady-state conditions, Chem. Eng. Sci. 192 (2018) 1124–1137, https://doi.org/10.1016/j.ces.2018.08.044.

[11] A. El Sibai, L.K. Rihko Struckmann, K. Sundmacher, Model-based optimal Sabatier reactor design for power-to-gas applications, Energy Technol. 5 (6) (2017) 911–921, https://doi.org/10.1002/ente.201600600.

[12] J. Bremer, K. Sundmacher, Operation range extension via hot-spot control for catalytic CO2 methanation reactors, React. Chem. Eng. 4 (6) (2019) 1019–1037, https://doi.org/10.1039/C9RE00147F.

[13] S.M. Biollaz, T.J. Schildhauer (Eds.), Synthetic Natural Gas from Coal, Dry Biomass, and Power-to-Gas Applications, John Wiley & Sons Inc, Hoboken, New Jersey, 2016.

[14] M.M. Quina, R.M. Ferreira, Start-up and wrong-way behavior in a tubular reactor: dilution effect of the catalytic bed, Chem. Eng. Sci. 55 (18) (2000) 3885–3897, https://doi.org/10.1016/S0009-2509(00)00029-4.

[15] L. Kiewidt, J. Thöming, Pareto-optimal design and assessment of monolithic sponges as catalyst carriers for exothermic reactions, Chem. Eng. J. 359 (2019) 496–504, https://doi.org/10.1016/j.cej.2018.11.109.

[16] S.K. Mazidi, M.T. Sadeghi, M.A. Marvast, Optimization of fischer-tropsch process in a fixed-bed reactor using non-uniform catalysts, Chem. Eng. Technol. 36 (1) (2013) 62–72, https://doi.org/10.1002/ceat.201200268.

[17] H. Wu, Q. Yuan, B. Zhu, An experimental investigation of optimal active catalyst distribution in nonisothermal pellets, Ind. Eng. Chem. Res. 27 (7) (1988) 1169–1174, https://doi.org/10.1021/ie00079a014.

[18] H. Wu, Q. Yuan, B. Zhu, An experimental study of optimal active catalyst distribution in pellets for maximum selectivity, Ind. Eng. Chem. Res. 29 (9) (1990) 1771–1776, https://doi.org/10.1021/ie00105a006.

[19] R. Aris, The Mathematical Theory of Diffusion and Reaction in Permeable Catalysts: The theory of the steady state, The Mathematical Theory of Diffusion and Reaction in Permeable Catalysts, Clarendon Press, 1975.

[20] M. Morbidelli, A. Gavriilidis, A. Varma, Catalyst Design, Cambridge University Press, Cambridge, 2001, https://doi.org/10.1017/CBO9780511721762.

[21] L. Jürgensen, E.A. Ehimen, J. Born, J.B. Holm-Nielsen, Dynamic biogas upgrading based on the sabatier process: thermodynamic and dynamic process simulation, Bioresour. Technol. 178 (2015) 323–329, https://doi.org/10.1016/j.biortech.2014.10.069.

[22] J.H. Ghouse, T.A. Adams, A multi-scale dynamic two-dimensional heterogeneous

model for catalytic steam methane reforming reactors, Int. J. Hydrogen Energy 38 (24) (2013) 9984–9999, https://doi.org/10.1016/j.ijhydene.2013.05.170.
[23] K.L. Fischer, M.R. Langer, H. Freund, Dynamic carbon dioxide methanation in a wall-cooled fixed bed reactor: comparative evaluation of reactor models, Ind. Eng. Chem. Res. 58 (2019) 19406 - 19420, doi:10.1021/acs.iecr.9b02863.
[24] P. Harriott, Thermal conductivity of catalyst pellets and other porous particles, Chem. Eng. J. 10 (1) (1975) 65–71, https://doi.org/10.1016/0300-9467(75)88018-X.
[25] F. Koschany, D. Schlereth, O. Hinrichsen, On the kinetics of the methanation of carbon dioxide on coprecipitated NiAl(O)x, Appl. Catal. B: Environ. 181 (2016) 504–516, https://doi.org/10.1016/j.apcatb.2015.07.026.
[26] J. Xu, G.F. Froment, Methane steam reforming, methanation and water-gas shift: I. Intrinsic kinetics, AIChE J. 35 (1) (1989) 88–96, https://doi.org/10.1002/aic.690350109.
[27] B. Kreitz, J. Friedland, R. Güttel, G.D. Wehinger, T. Turek, Dynamic methanation of CO2 – effect of concentration forcing, Chem. Ing. Tech. 91 (5) (2019) 576–582, https://doi.org/10.1002/cite.201800191.
[28] J. Bremer, K.H.G. Rätze, K. Sundmacher, CO2 methanation: optimal start-up control of a fixed-bed reactor for power-to-gas applications, AIChE J. 63 (1) (2017) 23–31, https://doi.org/10.1002/aic.15496.
[29] VDI-Wärmeatlas: Mit 320 Tabellen, 11th Edition, VDI-Buch, Springer Vieweg, Berlin, 2013.https://doi.org/10.1007/978-3-642-19981-3.
[30] E.L. Oliveira, C.A. Grande, A.E. Rodrigues, Methane steam reforming in large pore catalyst, Chem. Eng. Sci. 65 (5) (2010) 1539–1550, https://doi.org/10.1016/j.ces.2009.10.018.
[31] J. Ducamp, A. Bengaouer, P. Baurens, Modelling and experimental validation of a CO2 methanation annular cooled fixed-bed reactor exchanger, Can. J. Chem. Eng. 95 (2) (2017) 241–252, https://doi.org/10.1002/cjce.22706.
[32] J. Moulijn, A. van Diepen, F. Kapteijn, Catalyst deactivation: is it predictable? Appl. Catal. A: General 212 (1–2) (2001) 3–16, https://doi.org/10.1016/S0926-860X(00)00842-5.
[33] J.N. Armor, Do you really have a better catalyst? Appl. Catal. A: General 282 (1–2) (2005) 1–4, https://doi.org/10.1016/j.apcata.2005.01.014.
[34] N. Epstein, On tortuosity and the tortuosity factor in flow and diffusion through porous media, Chem. Eng. Sci. 44 (3) (1989) 777–779, https://doi.org/10.1016/0009-2509(89)85053-5.
[35] W.H. Ray, Non-isothermal catalyst particle performance under selective deactivation, Chem. Eng. Sci. 27 (3) (1972) 489–495, https://doi.org/10.1016/0009-2509(72)87004-0.
[36] R. Try, A. Bengaouer, P. Baurens, C. Jallut, Dynamic modeling and simulations of the behavior of a fixed-bed reactor-exchanger used for CO2 methanation, AIChE J. 64 (2) (2018) 468–480, https://doi.org/10.1002/aic.15874.
[37] G.F. Froment, K.B. Bischoff, J. de Wilde, Chemical Reactor Analysis and Design, third ed., John Wiley & Sons, Incorporated, 2010.
[38] B.E. Poling, J.M. Prausnitz, J.P. O'Connell, The Properties of Gases and Liquids, McGraw Hill Professional, McGraw-Hill Education, 2000.
[39] N. Wakao, T. Funazkri, Effect of fluid dispersion coefficients on particle-to-fluid mass transfer coefficients in packed beds, Chem. Eng. Sci. 33 (10) (1978) 1375–1384, https://doi.org/10.1016/0009-2509(78)85120-3.
[40] N. Wakao, S. Kaguei, T. Funazkri, Effect of fluid dispersion coefficients on particle-to-fluid heat transfer coefficients in packed beds, Chem. Eng. Sci. 34 (3) (1979) 325–336, https://doi.org/10.1016/0009-2509(79)85064-2.
[41] G.F. Froment, Fixed bed catalytic reactors—current design status, Ind. Eng. Chem. 59 (2) (1967) 18–27, https://doi.org/10.1021/ie50686a006.
[42] S. Yagi, D. Kunii, Studies on effective thermal conductivities in packed beds, AIChE J. 3 (3) (1957) 373–381, https://doi.org/10.1002/aic.690030317.
[43] H. Martin, M. Nilles, Radiale Wärmeleitung in durchströmten Schüttungsrohren, Chem. Ing. Tech. 65 (12) (1993) 1468–1477, https://doi.org/10.1002/cite.330651206.
[44] P.S. Nashtaee, B. Khoshandam, Noncatalytic gas-solid reactions in packed bed reactors: a comparison between numerical and approximate solution techniques, Chem. Eng. Commun. 201 (1) (2014) 120–152, https://doi.org/10.1080/00986445.2013.763229.
[45] J. Andersson, A general-purpose software framework for dynamic optimization (PhD thesis), Arenberg Doctoral School, KU Leuven, Department of Electrical Engineering (ESAT/SCD) and Optimization in Engineering Center, Kasteelpark Arenberg 10, 3001-Heverlee, Belgium, 2013.
[46] A.C. Hindmarsh, P.N. Brown, K.E. Grant, S.L. Lee, R. Serban, D.E. Shumaker, C.S. Woodward, Sundials: suite of nonlinear and differential/algebraic equation solvers, ACM Trans. Math. Software 31 (3) (2005) 363–396.
[47] A. Wächter, L.T. Biegler, On the implementation of an interior-point filter line-search algorithm for large-scale nonlinear programming, Math. Program. 106 (1) (2006) 25–57, https://doi.org/10.1007/s10107-004-0559-y.